Coupled cryoconite ecosystem structure–function relationships are revealed by comparing bacterial communities in alpine and Arctic glaciers

Edwards, Arwyn; Mur, Luis; Girdwood, Susan; Anesio, Alexandre Magno; Stibal, Marek; Edwards Rassner, Sara; Hell, Katherina; Pachebat, Justin; Post, Barbara; Bussell, Jennifer Sian; Cameron, Simon; Griffith, Gareth; Hodson, Andrew J.; Sattler, Birgit

Published in:
FEMS Microbiology Ecology

DOI:
10.1111/1574-6941.12283

Publication date:
2014

Citation for published version (APA):
Edwards, A., Mur, L., Girdwood, S., Anesio, A. M., Stibal, M., Edwards Rassner, S., Hell, K., Pachebat, J., Post, B., Bussell, J. S., Cameron, S., Griffith, G., Hodson, A. J., & Sattler, B. (2014). Coupled cryoconite ecosystem structure–function relationships are revealed by comparing bacterial communities in alpine and Arctic glaciers. *FEMS Microbiology Ecology*, *89*(2), 222-237. https://doi.org/10.1111/1574-6941.12283

RESEARCH ARTICLE

Coupled cryoconite ecosystem structure–function relationships are revealed by comparing bacterial communities in alpine and Arctic glaciers

Arwyn Edwards[1], Luis A.J. Mur[1], Susan E. Girdwood[1], Alexandre M. Anesio[2], Marek Stibal[3,4], Sara M.E. Rassner[1], Katherina Hell[5], Justin A. Pachebat[1], Barbara Post[5], Jennifer S. Bussell[1], Simon J.S. Cameron[1], Gareth Wyn Griffith[1], Andrew J. Hodson[6] & Birgit Sattler[5]

[1]Institute of Biological, Rural and Environmental Sciences, Aberystwyth University, Aberystwyth, UK; [2]Bristol Glaciology Centre, School of Geographical Sciences, University of Bristol, Bristol, UK; [3]Department of Geochemistry, Geological Survey of Denmark and Greenland, University of Copenhagen, Copenhagen, Denmark; [4]Centre for Permafrost, University of Copenhagen, Copenhagen, Denmark; [5]Institute of Ecology and Austrian Institute of Polar Research, University of Innsbruck, Innsbruck, Austria; and [6]Department of Geography, University of Sheffield, Sheffield, UK

Correspondence: Arwyn Edwards, Institute of Biological, Environmental and Rural Sciences, Cledwyn Building, Aberystwyth University, Aberystwyth SY23 3FG, UK. Tel.: +44(0)1970 622330; e-mail: aye@aber.ac.uk

Received 24 October 2013; revised 23 December 2013; accepted 7 January 2014. Final version published online 5 February 2014.

DOI: 10.1111/1574-6941.12283

Editor: John Priscu

Keywords
cryoconite; glacier; Svalbard; Greenland; Tyrol; metabolome.

Abstract

Cryoconite holes are known as foci of microbial diversity and activity on polar glacier surfaces, but are virtually unexplored microbial habitats in alpine regions. In addition, whether cryoconite community structure reflects ecosystem functionality is poorly understood. Terminal restriction fragment length polymorphism and Fourier transform infrared metabolite fingerprinting of cryoconite from glaciers in Austria, Greenland and Svalbard demonstrated cryoconite bacterial communities are closely correlated with cognate metabolite fingerprints. The influence of bacterial-associated fatty acids and polysaccharides was inferred, underlining the importance of bacterial community structure in the properties of cryoconite. Thus, combined application of T-RFLP and FT-IR metabolite fingerprinting promises high throughput, and hence, rapid assessment of community structure–function relationships. Pyrosequencing revealed *Proteobacteria* were particularly abundant, with *Cyanobacteria* likely acting as ecosystem engineers in both alpine and Arctic cryoconite communities. However, despite these generalities, significant differences in bacterial community structures, compositions and metabolomes are found between alpine and Arctic cryoconite habitats, reflecting the impact of local and regional conditions on the challenges of thriving in glacial ecosystems.

Introduction

Glaciers and ice sheets currently sequester *c.* 70% of Earth's freshwater (Shiklomanov, 1993). However, their roles as microbial habitats and their consequent *de facto* status as the largest freshwater ecosystems (Hodson *et al.*, 2008) on a planet subjected to repeated glaciations (Petit *et al.*, 1999) are less recognized.

Cryoconite is a dark microorganism-mineral aggregate that forms through interactions between microorganisms and dust deposited on glacial ice, leading to localized reduction in ice surface albedo and accelerated melting of ice in contact with cryoconite (Wharton *et al.*, 1985; Takeuchi *et al.*, 2001a,b; Langford *et al.*, 2010). The ensuing cylindrical melt holes are typically < 1 m in diameter and depth, growing downwards until an equilibrium depth is reached where downward growth rate equates surface ablation rates (Gribbon, 1979). Complex interactions between cryoconite, synoptic conditions and hydrology (Irvine-Fynn *et al.*, 2011) influence surface melting rates and hence glacial mass balance (Kohshima *et al.*, 1993; Fountain *et al.*, 2004).

Although the presence of organic matter in cryoconite has been known for over a century (Bayley, 1891), recognition of its importance in both glacial and microbial dynamics is more recent (Takeuchi *et al.*, 2001a,b; Takeuchi, 2002), leading to interactions between glacier surfaces and microbial processes (Stibal *et al.*, 2012a). Cryoconite

FEMS MICROBIOLOGY ECOLOGY

harbours diverse viral, archaeal, bacterial, microeukaryote and meiofaunal life (Desmet & Vanrompus, 1994; Säwström *et al.*, 2002; Edwards *et al.*, 2011; Cameron *et al.*, 2012a,b; Edwards *et al.*, 2013a). Remarkable rates of primary production and respiration, sometimes approaching those of temperate soils, have been associated with cryoconite ecosystems (Hodson *et al.*, 2007; Anesio *et al.*, 2009; Telling *et al.*, 2012a). Furthermore, cryoconite microorganisms interact with mineral debris to stabilize cryoconite granules (Hodson *et al.*, 2010; Langford *et al.*, 2010) and thus contribute to the formation of cryoconite stable over several seasons of growth (Takeuchi *et al.*, 2010; Irvine-Fynn *et al.*, 2011).

Hitherto, molecular exploration of cryoconite microbial diversity has largely focused on the cryoconite of polar glaciers (Christner *et al.*, 2003; Foreman *et al.*, 2007; Edwards *et al.*, 2011, 2013a,c; Cameron *et al.*, 2012a,b; Zarsky *et al.*, 2013). The differences in cryoconite communities appear linked to the properties of the cryoconite debris (Telling *et al.*, 2012a), in relation to glacier-specific factors (Edwards *et al.*, 2011, 2013a,c), but overall, interactions between diversity, functionality and cryoconite properties on regional to global scales remain poorly understood.

Fewer studies have examined the properties of cryoconite on mountain glaciers than polar glaciers despite the importance of surface dusts such as cryoconite in mountain glacier mass balance (Oerlemans *et al.*, 2009), carbon cycling (Anesio *et al.*, 2010) and its accumulation of radionuclide contaminants (Tieber *et al.*, 2009). Considering the concern for the fate of mountain glaciers and corresponding implications for water security in both mountain regions and arid regions fed by rivers containing glacial meltwaters (Barnett *et al.*, 2005; Kaltenborn *et al.*, 2010), comparative study of mountain glacier and polar cryoconite ecosystems is merited.

Previously, Xu *et al.* (2009) reported in detail the organic composition of debris from a single cryoconite hole on a glacier in the Rocky Mountains, and Hamilton *et al.* (2013) compared a single cryoconite site to other habitats associated with a glacier in the Rocky Mountains in terms of total and active community composition. We contend there is a paucity of information on the properties of cryoconite organic matter and microbial community structure from mountain glaciers. In particular, studies of European alpine cryoconite diversity have hitherto been limited to culture-dependent studies (Margesin *et al.*, 2002; Kim *et al.*, 2012). Recently, Edwards *et al.* (2013b) presented a 1.2 Gbp metagenome assembly from pooled cryoconite sampled on Rotmoosferner in the Austrian Alps. The assembly was dominated by the bacterial phyla *Proteobacteria, Bacteroidetes* and *Actinobacteria* followed by *Cyanobacteria*. *Archaea* and *Eukarya* were less abundant. Functional analyses highlighted the importance of stress responses and efficient carbon and nutrient recycling, consistent with subsistence on allochthonous organic matter.

Consequently, in this study, we sought to compare the bacterial communities of cryoconite ecosystems on alpine and Arctic glaciers and explore how they relate to cryoconite ecosystem functionality. To do so, we examined bacterial community structure with both T-RFLP analysis (Liu *et al.*, 1997) and barcoded amplicon 454 - pyrosequencing of bacterial 16S rRNA genes (Sogin *et al.*, 2006) and to relate these data to the biochemical properties of organic matter as assessed by metabolite fingerprinting using FT-IR spectroscopy.

Materials and methods

Study regions and sampling strategy

Debris (*c.* 5–10 g fresh weight) from randomly selected cryoconite holes in the ablation zones of alpine and Arctic glaciers were collected aseptically and transferred on ice to field stations for frozen storage prior to transfer to the Aberystwyth laboratory frozen in insulated containers for archival at −80 °C awaiting laboratory analyses.

Logistical constraints relating to severely limited helicopter time meant individual, neighbouring cryoconite holes were pooled at each station of the 50 km Greenland transect to secure sufficient sample material. Edwards *et al.* (2011) demonstrated an absence of a distance-decay relationship of bacterial community similarity at small (intraglacier) scales for Arctic cryoconite; therefore, it is presumed the impact of pooling within station is minimized when comparing Greenland against the other sites.

The properties of samples and sites are listed in Table 1. The population of cryoconite holes sampled from Svalbard glaciers has been profiled by bacterial 16S T-RFLP (Edwards *et al.*, 2013a,b,c). The Svalbard glaciers in question [Austre Brøggerbreen (AB), Midtre Lovénbreen (ML) and Vestre Brøggerbreen (VB)] are well described in terms of microbiology and glaciology (e.g. Edwards *et al.*, 2011, 2013a,c; Telling *et al.*, 2012a) as are the activities of cryoconite ecosystems on the southwestern margin of the Greenland Ice Sheet (GR) as recently reported in detail (Stibal *et al.*, 2010, 2012b; Telling, *et al.*, 2012b; Yallop *et al.*, 2012). In the Alps, the sites comprised three temperate valley glaciers in the Tyrolean Alps of Austria, namely Rotmoosferner (RF) and Gaisbergferner (GF), neighbouring glaciers in the Ötztal Alps, and Pfaffenferner (PF) in the Stubaier Alps. A metagenome derived from the same cryoconite holes on RF has recently been described (Edwards *et al.*, 2013b).

Table 1. Inventory of samples and summary diversity indices for T-RFLP and 454-16S profiles resolved at the level of 1 base pair bins and 97% sequence identity, respectively; S = number of peaks/OTUs; H′ = Shannon diversity index (loge); G_{corr} = corrected Gini coefficient. Organic matter content was determined for sediments from holes selected for pyrosequencing. Values are mean ±1 standard deviation

Region	High Arctic (Svalbard)			Greenland ice sheet	European Alps (Tyrol)		
Glacier	AB	ML	VB	Leverett glacier	GF	PF	RF
Latitude	78°53′54″N	78°53′04″N	78°54′ 45″N	67°04′17″N – 67°07′ 36″N	46°49′50″N	46°57′42″N	42°49′17″N
Longitude	11°48′17″E	12°02′17″E	11°43′16″E	50°08′45″W – 49°00′ 36″W	11°03′59″E	11°08′01″E	11°02′47″E
Altitude bounds (m asl)	190–310	170–300	140–270	400–1190	2480–2590	2780–2880	2620–2660
T-RFLP profiles	10	9	6	4	6	10	12
T-RFLP mean *S*	22.9 ± 18.6	15.3 ± 7.3	24.7 ± 6.9	25.0 ± 14.7	21.7 ± 8.9	20.0 ± 5.5	18.5 ± 7.7
T-RFLP mean *H′*	2.62 ± 0.56	2.39 ± 0.39	2.84 ± 0.26	2.81 ± 0.41	2.78 ± 0.39	2.64 ± 0.27	2.63 ± 0.51
T-RFLP mean G_{corr}	0.42 ± 0.03	0.39 ± 0.03	0.41 ± 0.07	0.42 ± 0.08	0.37 ± 0.05	0.41 ± 0.07	0.36 ± 0.06
FT-IR profiles	10	9	6	4	6	10	12
454 data sets	2	2	2	4	2	2	2
454 - mean *S*	177.0 ± 158.4	318.0 ± 19.8	81.0 ± 71.0	205.2 ± 153.2	265.0 ± 72.1	239.0 ± 2.8	242.0 ± 11.3
454 - mean *H′*	3.76 ± 0.11	4.11 ± 0.12	3.56 ± 0.03	3.61 ± 1.18	4.03 ± 0.13	3.84 ± 0.15	4.4 ± 0.03
Mean% LOI	3.0 ± 2.8	5.6 ± 0.4	7.3 ± 0.9	9.8 ± 4.7	2.2 ± 2.2	2.4 ± 1.5	2.9 ± 2.7

For cryoconite holes subjected to pyrosequencing, organic content was estimated by the % loss of ignition of sediment dried at 105 °C for 48 h and then ashed using a muffle furnace at 400 °C overnight in predried, preweighed crucibles.

DNA extraction

Cryoconite debris was thawed and aliquoted for DNA and freeze-dried for metabolite analyses. Community DNA was extracted from *c.* 250 mg cryoconite debris (wet weight) using a Powersoil DNA Kit according to the manufacturer's instructions (MoBio, Inc., Solana, CA) with DNA eluted into 100 μL buffer C6. DNA extraction and pre-PCR manipulations were conducted in laminar flow hoods using aseptic methods and aerosol-resistant tips. All plasticwares were certified DNA free.

T-RFLP

Bacterial 16S rRNA gene-derived community structure profiles were obtained by terminal restriction fragment length polymorphism (T-RFLP) exactly as previously described (Edwards *et al.*, 2013c). Each cryoconite hole was treated as an experimental replicate. In brief, triplicate PCR was conducted using a primer pair consisting of Cy5 fluorochrome tagged 27F (Cy5-5′-AGAGTTTGATC-CTGGCTCAG-3′) with the 1389R primer (5′-ACGGG-CGGTGTGTACAAG-3′) on 2 μL of each DNA extract for 30 cycles prior to Exo-SAP clean-up and subsequent Hae-III restriction digestion for 5 h. Preanalysis clean-up of terminal restriction fragments (T-RFs) was conducted using PCR clean-up columns (NBS Biologicals, Ltd, Cambridge, UK). T-RFs were separated using a Beckman CEQ-8000 genetic analyser in *Frag4* mode. Fragment profiles were exported to MS EXCEL 2007 for reformatting prior to permutational analysis of variance (PERMANOVA) and canonical analysis of principal components (Anderson, 2001; Anderson & Willis, 2003) using PRIMER-6.1.12 & PERMANOVA+1.0.2 (Primer-E, Ltd, Ivybridge, UK). Summary indices were calculated using PRIMER-6.1.12 with the exception of corrected Gini coefficients, which were calculated manually as previously described (Edwards *et al.*, 2011). MINITAB 14.20 was used for univariate statistics.

Amplicon pyrosequencing

A subset of 16 DNA samples from Svalbard, Greenland and the Tyrolean Alps was subjected to 454 pyrosequencing of the V1–V3 region of the bacterial 16S rRNA gene using the 27F primer (with Roche B adaptor) and 357R (5′- CTGCTGCCTYCCGTA, 5′- tagged with the Roche A adaptor and MID barcode tags). A microlitre of DNA extract was used in 25 μL reactions containing 1× reaction buffer with 1.8 mM magnesium chloride, 200 μM dNTPs, 0.2 μM of each primer, 1.25 U FastStart High Fidelity Enzyme mix (Roche Biosystems, Burgess Hill, West Sussex, UK). Triplicate PCRs were conducted for 30 cycles of 30 s at 95 °C, 30 s at 55 °C and 2 min at 72 °C prior to a final elongation of 7 min at 72 °C.

Amplicons were cleaned with Agencourt AMPure XP beads (Beckman Coulter Genomics, High Wycombe, UK) and pooled in equimolar concentrations prior to pyrosequencing with titanium chemistry and protocols on the

Aberystwyth Roche GS-FLX 454 sequencer (Roche Diagnostics Ltd, Burgess Hill, West Sussex, UK).

Sequences were demultiplexed, quality-filtered and analysed using QIIME (Caporaso *et al.*, 2010). Operational taxonomic units (OTUs) were assigned using UCLUST at a threshold of 97% pairwise identity, and representative sequences from each OTU selected for taxonomy assignment. These sequences were aligned using PYNAST and classified using the Ribosomal Database Project classifier against the RDP 16S rDNA core set using a 0.80 confidence threshold. The identity of OTUs not aligning to bacterial taxa was confirmed as (algal) plastids by alignment to the GreenGenes database as described previously (Hell *et al.*, 2013) and then excluded from analysis.

A matrix of each OTU's relative abundance in each sample (Table 1) was imported into PRIMER-6.1.12 & PERMANOVA+ for PERMANOVA and CAP and MINITAB 14.20 for correlation and univariate statistics as above. The full amplicon data set is available at EBI-SRA (PRJEB5067-ERP004426).

Metabolite fingerprinting by Fourier Transform Infrared spectroscopy

Cryoconite debris was flash-frozen using liquid nitrogen prior to freeze-drying overnight at −60 °C to stabilize material for FT-IR spectroscopy. One hundred milligram (dry weight; ±5 mg) subsamples of debris was disrupted by bead milling with steel ball bearings for 2 min at 30 Hz in a Retsch ball mill in sterile 2 mL microcentrifuge tubes, each containing 200 μL of a 1 : 2.5 : 1 admixture of chloroform, methanol and water; all reagents were HPLC-grade (Fisher Scientific, Loughborough UK). Metabolite extracts were clarified by centrifugation at 18 000 ***g*** at ambient temperature for 15 min.

FT-IR spectra of the mid infrared region (wavenumbers 4000–600 cm^{-1}) were acquired in reflectance mode at a resolution of *c.* 2 cm^{-1} using a Vertex 70 spectrometer (Bruker Optik, GmBH, Germany) equipped with a mercury–cadmium–telluride detector cooled by liquid nitrogen. Five microlitres of each sample was aliquoted onto 96-well reusable silicon sample carrier plates (Bruker Optics Ltd, Banner Lane, Coventry, UK) and oven dried at 50 °C for 30 min (Sanyo Gallenkamp plc., Loughborough, UK) to remove extraneous moisture. Prepared plates were inserted onto the motorized high-throughput stage (HTS) connected to the FT-IR spectrometer and immediately assayed. Spectra were derived from the average of 256 scans for each sample. The sample's absorbance spectrum was calculated from the ratio of I_S/I_R, where I_S was the intensity of the IR beam after it has been absorbed by the sample, and I_R was the intensity of the IR beam from the reference. The absorbance spectrum was therefore calculated as $-\log_{10}(I_S/I_R)$. Multivariate analyses employed PYCHEM software (Jarvis *et al.*, 2006).

To examine the influence of bacterial community structure on FT-IR-derived metabolite fingerprints, the absorbance spectra, each consisting of all 1762 data points, were imported to MVSP 3.1 (Kovach Computer Services, Ltd, Sir Fôn, Wales, UK) along with the cognate T-RF relative abundance profiles for each sample. Canonical correspondence analysis (CCA; Braak, 1986) was conducted using the Hill algorithm with multiple iterations to exclude environmental variables (T-RFs) incurring high variance inflation factors. Separate CCA models were generated for each glacier to minimize the length of environmental gradients ordinated. Finally, the application of distance-based redundancy analysis (dbRDA; Legendre & Anderson, 1999) using PRIMER-6.1.12 & PERMANOVA+1.0.2 permitted the exploration of an Euclidian distance matrix of taxon abundances from pyrosequencing data as predictor variables against absorbance spectra.

Results

T-RFLP profiles

T-RFLP profiles of bacterial 16S rRNA genes were successfully generated from all 57 samples from cryoconite holes in the seven locations described in Table 1. Terminal restriction fragments (T-RFs) were assumed to equate to phylotypes (*sensu* Prosser, 2012). There were no significant differences in T-RF peak number, Shannon diversity index or corrected Gini coefficient (Table 1) for T-RFLP profiles from different glaciers by one-way ANOVA (data not shown), suggesting a similar extent of bacterial community 'richness' and functional organization as described by the Gini coefficient (Wittebolle *et al.*, 2009; Edwards *et al.*, 2011) across all locations, with the caveat that T-RFLP may not resolve all taxa present in a sample (Blackwood *et al.*, 2007).

However, multivariate analyses showed that bacterial community structure differed among locations. Permutational multivariate analysis of variance (Anderson, 2001; PERMANOVA) provides a robust means of analysing multivariate diversity data such as that generated by T-RFLP or pyrosequencing. PERMANOVA was applied to test for interglacier differences and interregional differences in fourth-root transforms of Bray–Curtis distances between the T-RF relative abundance profiles of samples as a proxy for bacterial community structure. There were highly significant differences between glaciers (pseudo-$F = 8.98$; $P(\text{perm}) = 0.0001$) and between regions (pseudo-$F = 13.41$; $P(\text{perm}) = 0.0001$). The results of pairwise PERMANOVA tests which illustrate interglacier differences are summarized in Table 2. Strong support for

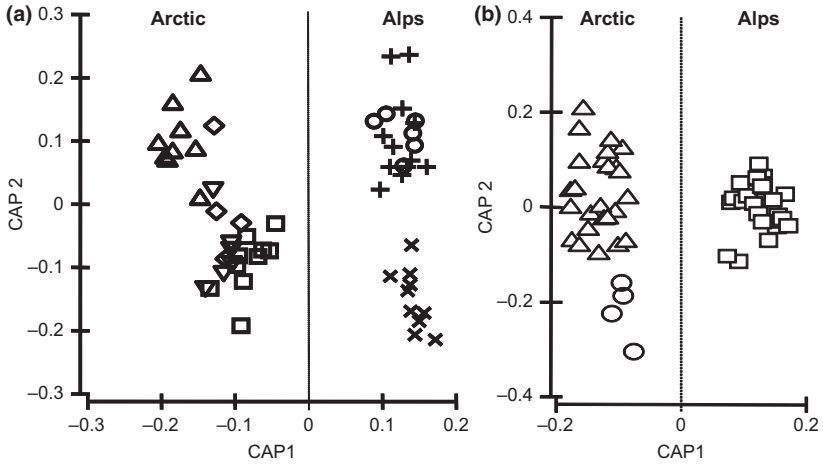

Fig. 1. Canonical analysis of principal components of T-RFLP modelled by (a) glacier (ML = triangles, VB = inverted triangles, AB = squares, GR = diamonds, GF = circles, PF = crosses, RF = pluses; total misclassification error = 19.3%) and (b) region (SV = triangles, GR = circles, AT = squares; total misclassification error = 5.3%).

Table 2. Pairwise PERMANOVA comparison *P* value results for individual glaciers' T-RFLP profiles. All values significant at $P < 0.01$ are highlighted in bold

	ML	VB	AB	GR	GF	RF	PF
ML	*	2.43	2.67	2.36	6.00	4.21	4.73
VB	**0.0004**	*	1.79	1.53	3.75	2.78	3.08
AB	**0.0001**	**0.005**	*	1.90	3.75	2.85	2.80
GR	**0.0014**	0.0186	**0.0014**	*	3.51	2.31	2.86
GF	**0.0001**	**0.0026**	**0.0002**	**0.0052**	*	2.16	2.70
RF	**0.0001**	**0.0003**	**0.0001**	**0.0006**	**0.001**	*	1.70
PF	**0.0002**	**0.0002**	**0.0001**	**0.0007**	**0.0003**	**0.0029**	*

differences between alpine and Arctic glaciers was obtained by pairwise tests (Svalbard vs. Austria = $P = 0.0001$; Greenland vs. Austria = $P = 0.0002$), while differences between Svalbard and Greenland glaciers are less striking ($P = 0.0132$). Because the parallel application of PERMANOVA and the related, constrained ordination method canonical analysis of principal components (CAP) is advocated (Anderson, 2001; Anderson & Willis, 2003), CAP was performed following PERMANOVA. Under models specified by glacier or region, strong support for differences between locations is provided by the CAP ordination and the model validations as summarized in Fig. 1.

Amplicon pyrosequencing

A total of 74 597 GS-FLX reads (16 samples in total; two cryoconites per glacier and four for the single Greenland glacier) corresponding to 616 operational taxonomic units (OTUs) clustered at the 97% sequence identity level at an abundance of ≥ 5 reads in the data set survived processing using the QIIME pipeline (Caporaso *et al.*, 2010). For a full list of genera present in the samples, the reader is directed to Supporting Information, Table S1. In a manner similar to T-RFLP profiles, no significant differences between OTU richness and Shannon diversity index were identified by glacier or correlated with organic matter as calculated by % loss of ignition (Table 1), but regional comparisons were made of the relative abundance profiles of OTUs using PERMANOVA and CAP. PERMANOVA returned highly significant interregional differences in bacterial community composition (pseudo$F = 3.99$; P(perm) = 0.0002) entirely due to differences between Arctic and alpine locations (pairwise PERMANOVA: Svalbard vs. Greenland, $P = 0.184$; Svalbard vs. Tyrol, $P = 0.0016$; Greenland vs. Tyrol, $P = 0.0055$). Similarly, CAP highlights regional differences (Fig. 2) as it assigns 94.7% of samples to the correct regional group.

Analysis of the OTUs aligned and assigned to the RDP core set to the level of phyla or proteobacterial class at a confidence of 0.80 or more retained a consistent effect of region (Table 3), with significant or highly significant differences between Svalbard and Tyrol in terms of OTU composition for all phyla (plus proteobacterial classes) with the exception of *Gammaproteobacteria* revealed by pairwise PERMANOVA. Similarly, significant differences were apparent between Greenland and Tyrol cryoconites with the exception of *Cyanobacteria* ($P = 0.084$), *Firmicutes, Gammaproteobacteria* and TM7. In stark contrast, no significant differences are apparent between Greenland and Svalbard at the level of 97% sequence identity OTUs for any of the phyla or classes tested by PERMANOVA.

At the highest taxonomic levels, this effect is somewhat diminished; however, univariate analysis of summed relative abundances for high-rank taxa returned highly significant differences in the relative abundances of some of the dominant high-ranked taxa. *Proteobacteria* predominate the cryoconite communities profiled by pyrosequencing. Sequences assigned to unclassified *Proteobacteria, Alphaproteobacteria* and *Betaproteobacteria* are highly

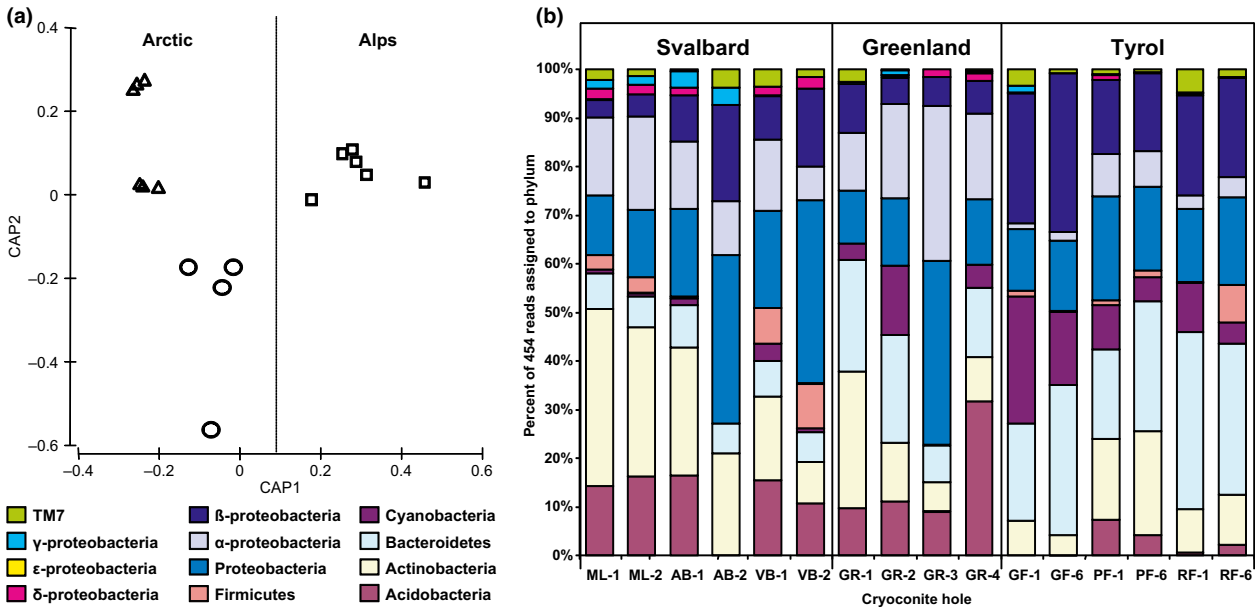

(c)

		Acidobacteria	*Actinobacteria*	*Bacteroidetes*			*Cyanobacteria*	*Firmicutes*			*Proteobacteria*						TM7
Region	Site	*Acidobacteria*	*Actinobacteria*	*Sphingobacteria*	*Flavobacteria*	Other		*Bacilli*	*Clostridia*	*Other*	*Alpha-*	*Beta-*	*Delta-*	*Epsilon-*	*Gamma-*	Other	
Svalbard	ML-1	14.13	36.31	3.76	0.22	3.29	0.65	0.07	2.93	0	15.82	3.72	2.31	0	1.66	12.90	2.20
Svalbard	ML-2	16.22	30.60	3.34	0.08	2.97	0.68	0.15	3.08	0.11	19.26	4.54	1.95	0	1.69	13.78	1.46
Svalbard	AB-1	16.02	25.72	4.30	0.49	3.68	1.41	0.06	0.43	0	13.44	9.33	1.47	0	3.44	19.71	0.31
Svalbard	AB-2	0	20.00	4.71	1.18	0	0	0	0	0	10.59	18.82	0.00	0	3.53	32.94	3.53
Svalbard	VB-1	14.66	16.38	2.59	2.59	1.72	3.45	1.72	4.31	0.86	13.79	8.62	1.72	0	0	19.83	3.45
Svalbard	VB-2	10.29	8.09	2.94	0	2.94	0.74	0.00	5.88	2.94	6.62	15.44	2.21	0	0	36.03	1.47
Greenland	GR-1	9.73	28.06	20.19	0.14	2.61	3.38	0.02	0	0	11.88	10.06	0.09	0	0.26	10.76	2.65
Greenland	GR-2	11.06	12.04	15.25	0.64	6.30	14.19	0	0	0	19.17	5.47	0.49	0	1.06	13.89	0.15
Greenland	GR-3	8.00	5.33	4.00	1.33	1.33	0.00	0	0	0	28.00	5.33	1.33	0	0	33.33	0
Greenland	GR-4	31.64	8.96	4.12	0.27	9.82	4.84	0	0	0	17.47	6.70	1.63	0.05	0.41	13.26	0.36
Alps	GF-1	0	7.21	16.95	2.24	0.72	26.05	0.21	0.82	0.08	1.20	26.61	0.21	0.03	1.28	12.69	3.38
Alps	GF-6	0.02	4.21	29.59	1.01	0.12	15.03	0.00	0.02	0.05	1.75	32.42	0.00	0	0.12	14.56	0.76
Alps	PF-1	7.31	16.43	15.36	0.05	3.02	8.87	0.10	0.44	0.39	8.68	14.97	1.07	0	0.20	21.50	0.93
Alps	PF-6	4.24	21.24	22.52	0	3.84	4.98	0	0.64	0.59	7.29	15.77	0.15	0	0.10	17.30	0.59
Alps	RF-1	0.63	8.85	32.92	0	3.33	9.99	0	0	0.20	2.73	20.57	0.33	0	0.30	14.98	4.63
Alps	RF-6	2.29	10.19	22.54	0.08	8.17	4.34	0	5.13	2.61	4.18	20.17	0.20	0	0	17.84	1.58

Fig. 2. Barcoded amplicon 454 pyrosequencing of bacterial 16S rRNA genes. (a) Canonical analysis of principal components of UCLUST 97%-clustered OTUs modelled by region (total misclassification error = 6.25%; SV = triangles, GR = circles, AT = squares) (b) distribution of OTUs aligned and assigned to known bacterial phyla (c) heatmap of summed relative abundances of bacterial OTUs affiliated to known bacterial taxa revealed by 16S rRNA gene amplicon pyrosequencing. Cell values are the summed relative abundance of 97%-clustered OTU in each sample while each cell is coloured so that the sites comprising the lowest quartile of relative abundance of the taxon across the data set are coloured white, the second quartile light grey, the third quartile dark grey and the upper quartile shaded black.

Table 3. Statistical analysis of taxon relative abundance revealed by pyrosequencing at the level of UCLUST 97%-clustered OTUs analysed by PERMANOVA and summed relative abundance analysed by one-way ANOVA or Kruskal–Wallis; *P* values < 0.05 are shown in bold, while *P* values < 0.01 are also underlined to highlight significant and highly significant differences by region, respectively

	Overall changes in taxon relative abundance - univariate statistics			Changes in OTU relative abundance by taxon - PERMANOVA							
				Overall		Pairwise tests					
						Pairwise *t* statistics			Pairwise *P* value		
Taxon	Statistic*	*P*	Tukey's	Pseudo-*F*	*P*(Perm)	Sv × Gr	Sv × At	Gr × At	Sv × Gr	Sv × At	Gr × At
Acidobacterium	5.05	**0.024**	At X Gr	1.9883	**0.034**	0.79	1.63	1.45	0.513	**0.0169**	**0.03**
Actinobacterium	2.23	0.146	NT	1.9883	**0.034**	1.05	1.49	1.64	0.355	**0.0301**	**0.0043**
Bacteroidetes	11.76	**0.001**	At X Gr & Sv	2.9518	**0.002**	0.84	2.07	2.36	0.707	**0.0022**	**0.0054**
Cyanobacterium	4.85	**0.027**	At X Gr	4.1685	**0.0019**	1.51	2.6	1.43	0.143	**0.0025**	0.0829
Firmicutes	1.55	0.25	NT	3.8159	**0.0024**	1.52	2.08	2.1	0.165	**0.0136**	0.1427
Proteobacteria (unclassified)	1.28	0.526	NT	2.979	**0.0037**	1.15	1.99	1.98	0.238	**0.013**	**0.0048**
Alphaproteobacteria	16.76	**0.0001**	At X Gr & Sv	3.1021	**0.0005**	1.41	1.66	2.28	0.066	**0.0093**	**0.0102**
Betaproteobacteria	6.73	**0.01**	At X Gr & Sv	3.7726	**0.0004**	1.31	2.02	2.71	0.143	**0.0019**	**0.0049**
Deltaproteobacteria	4.51	0.33	NT	NT	NT	NT	NT	NT	NT	NT	NT
Gammaproteobacteria	2	0.175	NT	1.1736	0.3193	0.6	1.35	1.07	0.86	0.1498	0.3591
TM7	1.07	0.37	NT	2.2143	**0.0246**	1.24	2.12	0.47	0.159	**0.0052**	0.9571

*All tests one-factor ANOVA with exception of *Proteobacteria* (unclassified) which is Kruskal–Wallis.

abundant in the data sets (Fig. 2). Contrasts in the distributions of *Alphaproteobacteria* and *Betaproteobacteria* are very apparent, with a strongly negative correlation (Pearson's $r = 0.876$, $P = < 0.0001$) between the summed relative abundances of OTUs affiliated to each class. In Arctic locations, *Alphaproteobacteria* account for 15–28% of the reads affiliated to higher ranked taxa, yet only 1–9% of reads affiliated to higher ranked taxa in alpine locations; this is reflected in a highly significant difference (one-way ANOVA; $F = 16.7$, $P = 0.0001$). *Betaproteobacteria*, on the other hand, account for 4–19% of reads assigned to a bacterial taxon in Arctic locations, but 15–32% of reads assigned to a bacterial taxon in alpine locations.

Cyanobacterial sequences were poorly represented in the investigated Arctic locations, particularly on Svalbard, while cryoconites on alpine glaciers (in particular Gaisbergferner) harbour a greater abundance of cyanobacterial-affiliated sequences. In both instances, the relative abundance of cyanobacterial OTUs represented in the 454 data set was limited (Fig. 2) for habitats characterized by apparently high rates of primary production. This is consistent with prior clone library studies from Svalbard cryoconite (Edwards *et al.*, 2011) and shotgun metagenomes from alpine cryoconite (Edwards *et al.*, 2013b) or glacial ice (Simon *et al.*, 2009). A highly significant difference in the relative abundance of taxa affiliated with the phylum *Bacteroidetes* is also apparent between Austrian and Greenland and Svalbard locations (Table 3; one-way ANOVA $F = 11.76$, $P = 0.001$), which appears to be accounted for solely by a lower relative abundance of reads affiliated to the class *Sphingobacteria* on Svalbard glaciers compared with Austrian and Greenland locations (one-way ANOVA, $F = 9.91$, $P = 0.002$), whereas *Flavobacteria* and other *Bacteroidetes* lineages show no significant differences in distribution.

FT-IR metabolite fingerprints

Metabolite fingerprinting was employed based on FT-IR spectroscopy. The derived sample spectra had a relatively low absorbance but elevated absorbencies in wavenumbers linked to amides, and fatty acids were detected (Fig. 3a). Principal component analysis (PCA) of the derived spectra suggested separation between samples from alpine and Arctic cryoconites holes along PC1 explaining 80% of the variation (Fig. 3b). To further examine the sources of variation within the samples, discriminant function analysis (DFA) was employed. DFA is a supervised approach where assessments include *a priori* knowledge of the experimental classes, here seven classes representing the seven locations. DFA allowed the tight clustering of replicate samples within each class in all cases except the Svalbard glacier, ML. Separation between samples from alpine and Arctic cryoconite was observed along discriminant function 1 (DF1; Fig. 3c). The samples from the Greenland ice sheet cryoconite (GR) were distinctive to samples originating from Svalbard (AB, VB and ML). Plotting the loading vectors used in DFA to separate between alpine – Svalbard and Greenland samples indicated that fatty acid differences were a major source of variation (Fig. 3d).

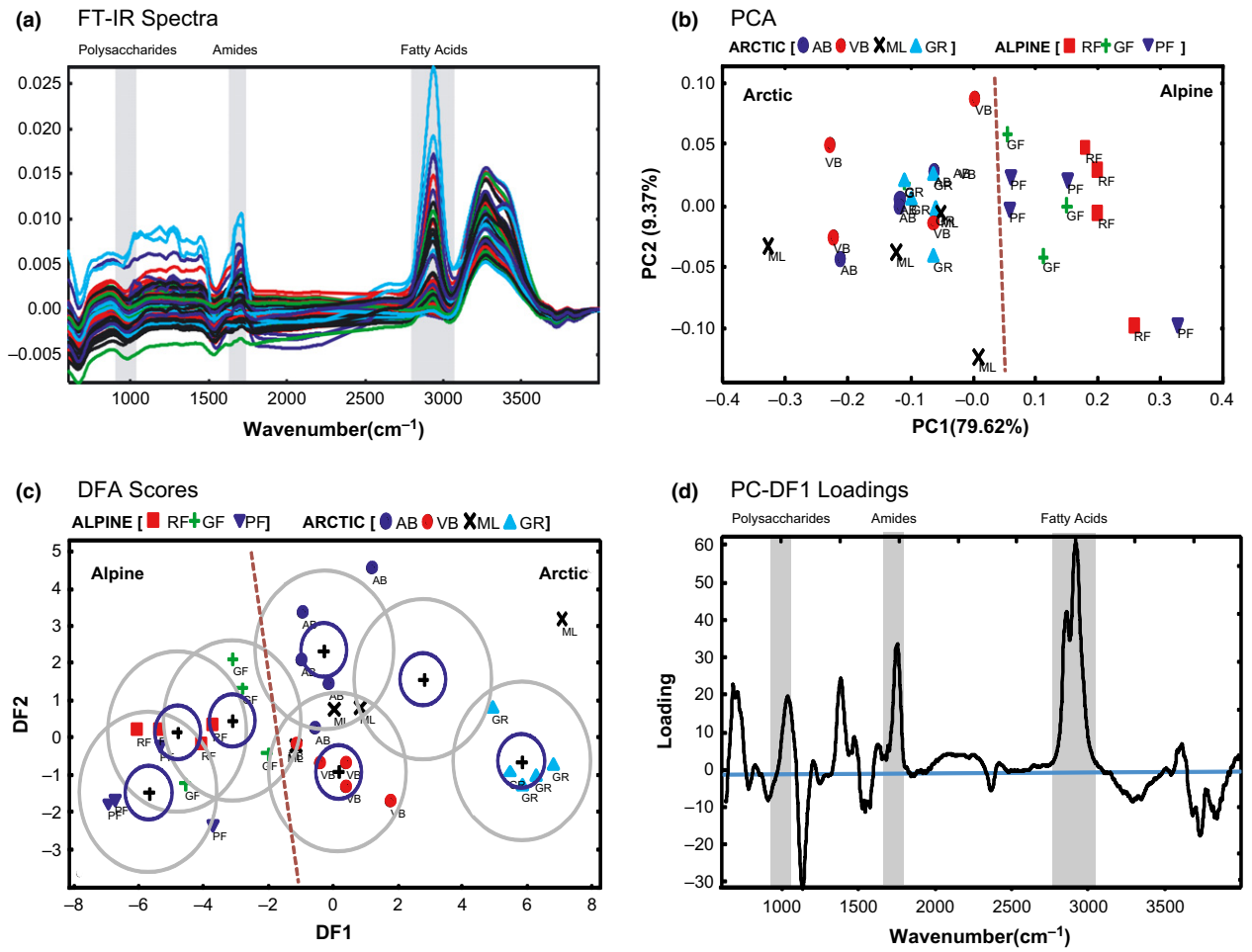

Fig. 3. Metabolite fingerprinting cryoconite samples by Fourier transform infrared spectroscopy. (a) Fourier transform infrared (FT-IR) spectra of cryoconite samples. Wavenumbers linked to absorption by polysaccharide, amide and fatty acid groups are indicated in grey. (b) Principal component analysis of FT-IR spectra derived for Arctic (AB; ML; VB; GR) and alpine (GF; PF; RF) glaciers. The dotted line indicates a separation of ordinants from Arctic and alpine glaciers along principal component [PC] 1 and is of no mathematical significance. (c) Discriminant function analysis of FT-IR spectra based on 4 PCs explaining 98.76% of the total variation. Seven *a priori* data classes are assigned, each class referring to samples from a single glacier. The crosses denote the mean values for each group, and the blue and grey circles represent 90% and 95% confidence intervals. The dotted line indicates a separation of ordinants from Arctic and alpine glaciers along discriminant function 1 (DF1) and is of no mathematical significance. (d) Loading vectors assigned to wavenumbers used to derive DF1 are indicted. The horizontal line indicates the position of wavenumbers if they are making no contribution to the model shown in (c). Wavenumbers linked to absorption by polysaccharide, amide and fatty acid groups are indicated in grey. Note that the main sources of variation contributing to the discrimination between Arctic and alpine samples are to be found in the fatty acid absorbencies.

Bacterial community structure interaction with cryoconite metabolite fingerprints

As bacterial community structure and cryoconite metabolite fingerprints appeared to vary in a coordinated manner, we used canonical correspondence analysis [CCA; (Braak, 1986)] to model the influence of T-RF relative abundance profiles on FT-IR spectra.

Following initial model generation, environmental variables (T-RFs) were excluded in a stepwise manner to eliminate multicollinearity and variance inflation to optimize each model's robustness. This approach was important to minimize the influence of interglacier and interregional differences, which could result in artificially elongated environmental gradients. Ordination plot summaries of CCA models for individual cryoconite holes for each glacier are displayed in Figs 4 and 5, respectively.

Some striking features are common to all CCA models. In particular, each model is constrained by just a few terminal restriction fragments, with the CCA model for Rotmoosferner (Fig. 5c) using eight T-RFs, whereas in other glaciers, only 2–4 T-RFs were retained in the optimized

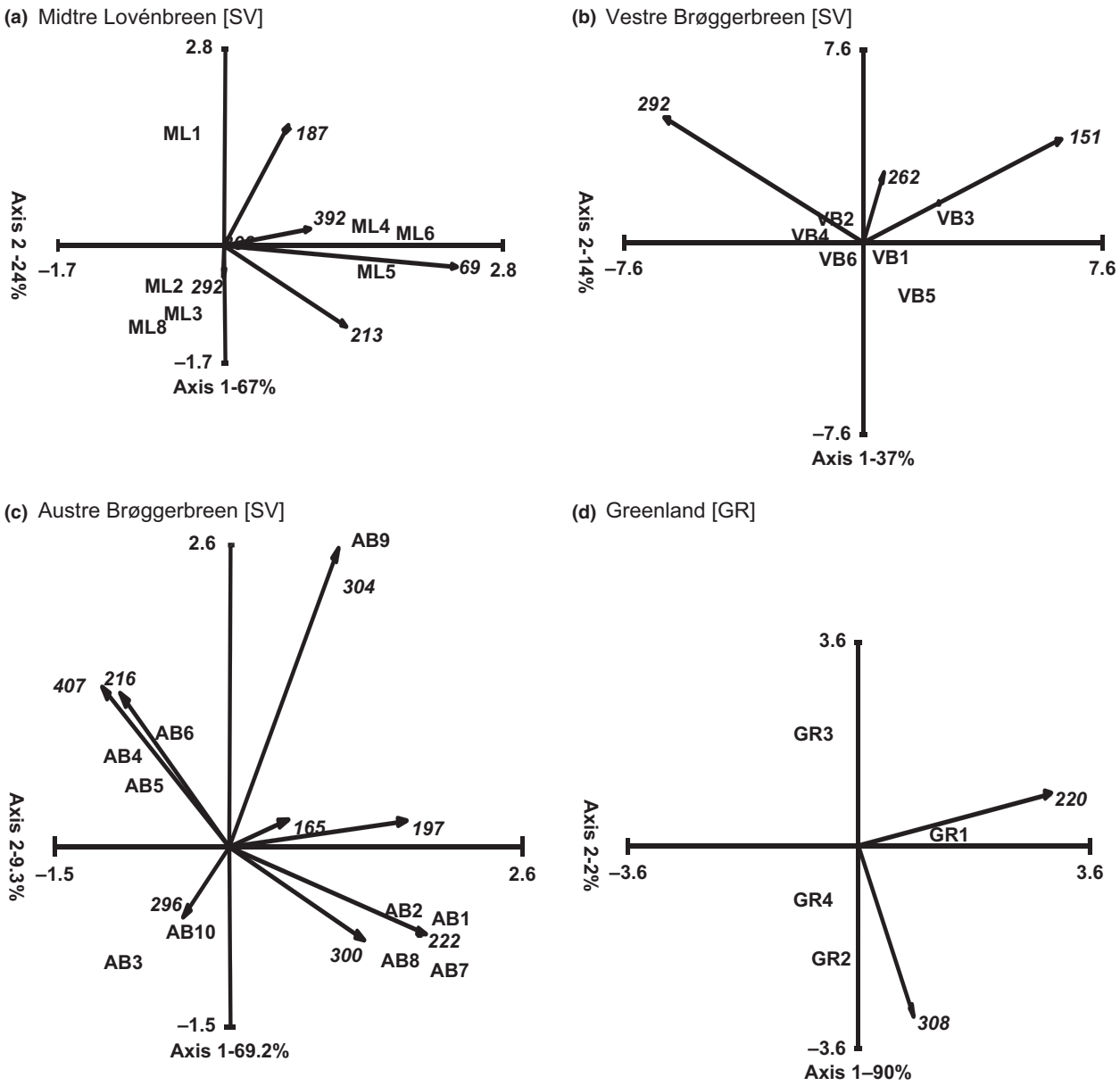

Fig. 4. Canonical correspondence analysis models of terminal restriction fragment relative abundance influence (vectors) on metabolite fingerprints (sites) for Arctic glaciers (a: AB; b: ML; c: VB; d: GR). Note each axis is labelled with the percentage of total variance in metabolite profile explained by T-RF profiles within that axis.

model (Fig. 5a and b). These T-RFs therefore account for considerable proportions of total variance within the metabolite profiles in the first two axes. In the most extreme example, two 27F-HaeIII-derived T-RFs (220 and 308 bp in length) account for 92% of the total variance in the metabolite profiles obtained from Greenland cryoconite in the first two axes. In this regard, the weakest model is that derived for the alpine glacier, Gaisbergferner, which still describes 51% of the total variance in metabolite profiles in the first two environmental axes.

The limited number of cryoconite holes subject to both pyrosequencing and FT-IR profiling precludes efficient canonical correlation analyses of OTUs and FT-IR spectra to permit direct identification of the taxa influencing the cryoconite metabolite fingerprints on a per-glacier basis. Nevertheless, two other options for such a comparison were explored. Firstly, putative matches of T-RFs represented in the optimized model to the predicted T-RF sizes of 16S rRNA clones recovered from Svalbard cryoconite, FN824532–FN824621 (Edwards *et al.*, 2011), were

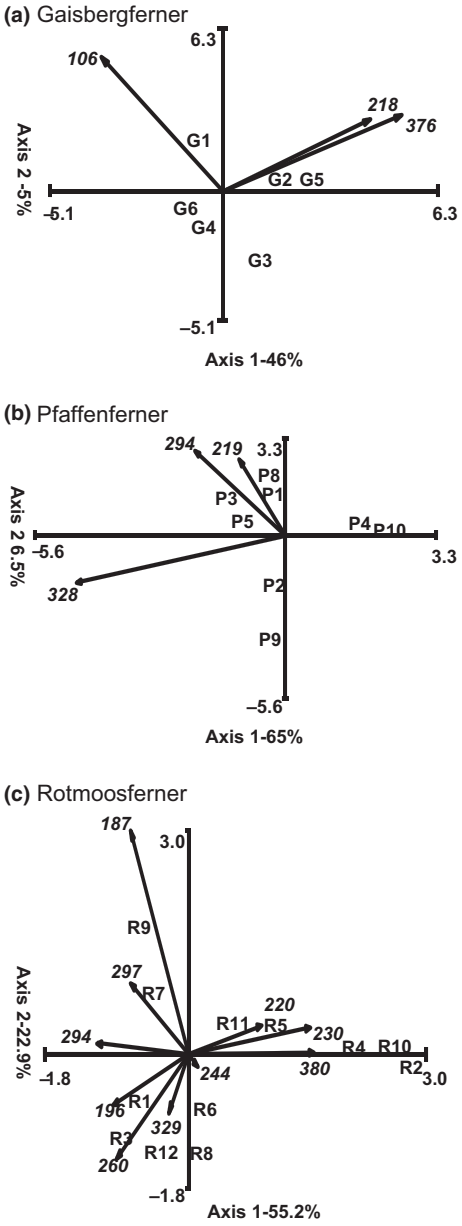

Fig. 5. Canonical correspondence analysis models of terminal restriction fragment relative abundance influence (vectors) on metabolite profiles (sites) for alpine glaciers (a: GF; b: PF; c: RF). Note each axis is labelled with the percentage of total variance in metabolite profile explained by T-RF profiles within that axis.

attempted. These yielded exact (=1 bp bin size) matches to 14 of 33 T-RFs exhibiting intraset correlations ≥ 0.1 for one or more of the first three environmental axes (i.e. T-RFs considerably weighting the axis). Similar to the pyrosequencing data sets, proteobacterial clones are predominant in these matches; however, cyanobacterial clones are also represented. Further details are given in Table S2. Finally, distance-based redundancy analysis was performed using the summed relative abundances presented in Fig. 2c as predictor variables against the FT-IR spectral data. The influence of *Alpha-* and *Beta-proteobacterial* classes was most apparent, with the dominant positive and negative loadings, respectively, on dbRDA1, which explains 77.6% of the total variation in metabolite profiles.

Discussion

This study reveals that alpine and Arctic cryoconite ecosystems are distinct in terms of community structure, OTU composition and metabolite profiles. Nevertheless, close correlation between community structure and metabolite profiles is apparent for all glaciers upon canonical correspondence analysis.

Arctic and alpine cryoconites are subject to differences in terms of day length and incident solar radiation, altitude, typical synoptic conditions and the nature of mass-transfer interactions with ice-marginal environments. As cryoconite holes act as crude indicators of glacier surface energy balance (McIntyre, 1984) and latitudinal gradients in maximal solar elevation have been thought to influence cryoconite hole development (Steinbock, 1936), cryoconite holes in lower latitudes may be less stable (McIntyre, 1984) when compared to those at higher latitudes (Nobles, 1960).

Furthermore, the potential Aeolian input is substantially different with the high diversity of vegetation in adjacent valleys, meadows and forests in alpine regions. However, previous work has shown the structure of (Svalbard) cryoconite bacterial communities is substantially different from ice-marginal habitats (Edwards *et al.*, 2013c). Whether Greenland or European alpine cryoconite communities, unlike Svalbard cryoconites, are structured by mass-transfer effects from Aeolian deposition from proximal habitats remains unknown and should be investigated further.

Pyrosequencing reveals the abundance of proteobacterial lineages within the cryoconite bacterial community (Fig. 2), consistent with clone library studies (Edwards *et al.*, 2011; Cameron *et al.*, 2012b) and high-throughput sequencing (Zarsky *et al.*, 2013) of polar cryoconite 16S amplicons, alpine cryoconite metagenome (Edwards *et al.*, 2013a,b,c), debris-covered glacier 16S amplicons (Franzetti *et al.*, 2013) and alpine glacial ice metagenome (Simon *et al.*, 2009). It may be that proteobacterial taxa in cryoconite are well-adapted to respond to frequent environmental fluctuations typical of short active seasons in extreme environments, while contributing to the mineralization of cryoconite carbon, exhibiting similar properties to terrestrial *Proteobacteria,* which are characterized by Fierer *et al.* (2007) as ruderal (*r*) strategists.

The strong negative correlation in the summed relative abundance of OTUs affiliated to the classes *Alphaproteobacteria* and *Betaproteobacteria* revealed by pyrosequencing is particularly striking and may indicate a degree of functional redundancy between the classes. The prominence of *Alphaproteobacteria* on the Arctic glaciers revealed in this study is supported by previous work on Svalbard cryoconite (Edwards *et al.*, 2011, 2013a,b,c), while *Betaproteobacteria* were more prevalent in the metagenome from Rotmoosferner cryoconite (Edwards *et al.*, 2013a,b,c).

These reciprocal patterns of alphaproteobacterial and betaproteobacterial abundance could relate to increased distance from marine sources at alpine sampling sites (> 200 km from the sea; Philippot *et al.*, 2010). However, amplicon pyrosequencing also reveals that adjoining habitats on Svalbard glaciers such as snow, slush and surface ice (Hell *et al.*, 2013) and meltwater (S.M.E. Rassner, unpublished data) are dominated by *Betaproteobacteria*. Similar transitions between *Alphaproteobacteria* and *Betaproteobacteria* have been associated with increasing community development in both glacial (Philippot *et al.*, 2011) and nonglacial (Jangid *et al.*, 2013) systems. Consequently, an alternative explanation is that the pattern reflects a transition between *Betaproteobacteria* and *Alphaproteobacteria* due to increasing cryoconite granulation and hence habitat stability or age, more typical of granular cryoconite frequently observed on Arctic ice masses relative to biofilm-coated mineral grains observed on the alpine glaciers sampled.

Clear interregional differences in the composition of the cryoconite metabolite fingerprints are also apparent. Langford *et al.* (2011) applied KBr-pellet FT-IR spectroscopy to characterize the mineralogy and geochemistry of 12 cryoconite holes on a glacier in Svalbard, documenting variation in the prevalence of carbohydrates in cryoconite organic matter. Although FT-IR spectroscopy is broadly used as a high-throughput metabolomic profiling method (Johnson *et al.*, 2004; Gidman *et al.*, 2006), capable of linking bacterial diversity with metabolite content even in soil environments (Scullion *et al.*, 2003; Elliott *et al.*, 2007), its application in glacial ecosystems is in its infancy. While targeted analyses of cryoconite carbohydrates have been reported (Stibal *et al.*, 2010), the detailed broad-spectrum profiling of cryoconite organic matter is more limited (Xu *et al.*, 2009; Pautler *et al.*, 2013), but reveal a range of microbial biomarkers and ascribing the presence of long-chain hydrocarbons to allochthonous transfers of vascular plant debris.

Here, we demonstrate that FT-IR spectroscopy reliably detected distinctive differences between cryoconite holes from alpine and Arctic samples, and within the latter class between Svalbard and Greenland (Fig. 3). The major sources of variation as suggested from DFA were mainly differences in fatty acids. Differences in microbial fatty acids are a well-established tool in chemotaxonomy (Vasyurenko & Frolov, 1986; Frisvad *et al.*, 2008); for example, rapidly resolving even intraspecific variation in bacterial isolates from Antarctic microbial mats (Tindall *et al.*, 2000). Our interpretation is that the fatty acid differences between geographical sites are likely to reflect variation in microbial community structure. Thus, FT-IR has suggested potential fatty acid biomarkers that could be linked to defined microbial populations and biological activities. Full metabolome mass spectrometric profiling will allow each biological activity to be defined, but the data that we have presented show that coupling of T-RFLP and FT-IR in this manner appears a promising tool for rapid high-throughput characterization of cryoconite (and other microbial ecosystem) properties.

Canonical correspondence analysis clearly resolves the interaction between bacterial community structure and FT-IR spectra, with intraglacier variation in metabolite profiles closely correlated with intraglacier variation in cryoconite bacterial T-RFLP profiles in all instances (Figs 4 and 5). Interregional variances are implied by the differential inclusion of T-RFs significantly influencing metabolite profile variation. This would imply that different bacterial taxa are closely correlated with the properties of cryoconite organic matter in different locations. The limited number of samples we could analyse using pyrosequencing precluded detailed comparison at the intraglacier scale between taxonomic and metabolic profile; however, dbRDA (Fig. 6) illustrates that at the interglacier and interregional scale, taxonomic composition of the bacterial community is a good predictor of metabolite profile composition. It is clear that the numerically dominant *Betaproteobacteria* and *Alphaproteobacteria* classes that display contrasting distributions between Alps and Arctic sites exert considerable influence on the metabolite profiles resolved by FT-IR.

When combined, our results are consistent with the contribution of bacteria resident in cryoconite to the cryoconite metabolite profile. Tracing the impact of specific taxa upon community metabolomes is often difficult, hindered by extensive functional redundancy in community composition, but may be achieved by multivariate analysis (Huws *et al.*, 2011), and comparable differences between T-RFLP and FT-IR profiles are noted in other systems with considerable levels of functional redundancy (Scullion *et al.*, 2003; Dougal *et al.*, 2012). As summarized in Table 1, in all cases, cryoconite communities displayed a moderate to high degree of functional organization as inferred by the corrected Gini coefficients of T-RFLP profiles, which represent a specific extent of evenness (Wittebolle *et al.*, 2009). This is consistent with

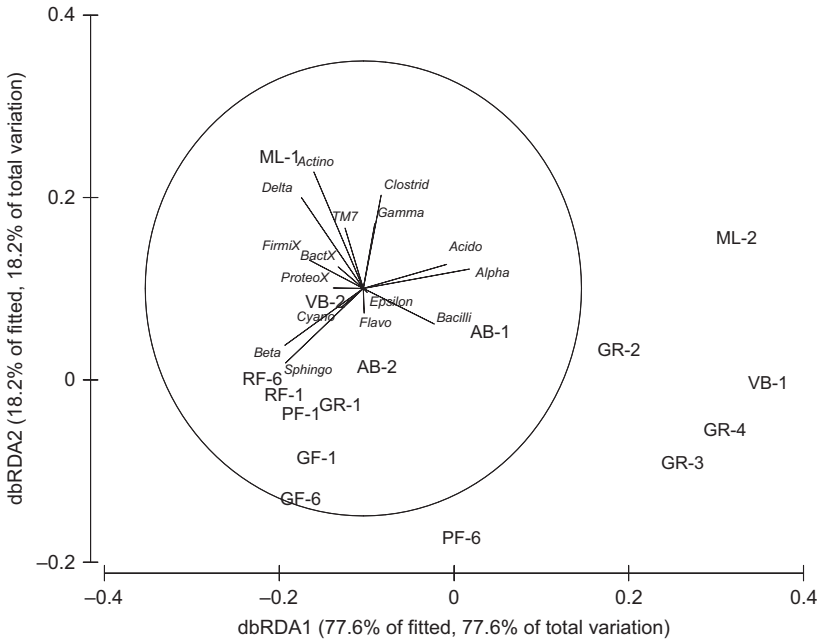

Fig. 6. Distance-based redundancy analysis model of taxon abundance (as reported in Fig. 2c) as a predictor variable on metabolite profiles for cryoconite holes with coupled pyrosequencing and FT-IR profile data. Note the cumulative high percentage of fitted and total variation explained within the first two axes. Congruent ordination between dbRDA and principal coordinates analyses indicated the robustness of the model generated (data not shown). Predictor variables key: Acido = *Acidobacteria;* Actino = *Actinobacteria;* Alpha-Epsilon = classes of *Proteobacteria*; BactX = Unclassified *Bacteroidetes*; Clostrid = *Clostridia;* Cyano = *Cyanobacteria;* FirmiX = Unclassified *Firmicutes;* Flavo = *Flavobacteria;* ProteoX = Unclassified *Proteobacteria;* Sphingo = *Sphingobacteria.*

previous findings for High Arctic cryoconite (Edwards *et al.*, 2011) and would indicate a comparatively reduced capacity overall for functional redundancy at a steady-state phylotype abundance distribution.

In this context, T-RFs contributing significantly to metabolite profiles are present among the dominant T-RF abundance distributions for different regions (Supporting Information, Fig. S1), but are also distributed along the longer tail of T-RF abundances.

Three possibilities may account for this. Firstly, the phylogenetic resolution of T-RFLP may not be consistent across the spectrum of bacterial diversity. In some instances, T-RFs are shared between some taxa, thus distorting equivalence between T-RF and taxon abundance (Blackwood *et al.*, 2007). Therefore, some dominant T-RFs may composite several taxa, one or more of which may be the source of influences from metabolite profiles, while less dominant T-RFs may represent resolved individual, lower-ranked taxa making significant contributions. Secondly, where the phylogenetic resolution of T-RFLP is consistent, this would indicate that rarer taxa in cryoconite may make important contributions to the cryoconite metabolite profile. This would be comparable with the conceptual model of Turnbaugh and Gordon (2008) for the disruption of partitioned contributions of modal and rare taxa to community metabolomes experiencing perturbations. Finally, it may be that taxa less well represented by 16S rRNA gene analyses may in fact be more active or possess a broader repertoire of metabolites. In either the second or third scenarios, such organisms could be considered keystone taxa within the community metabolome.

For cryoconite, the limited representation of cyanobacterial 16S rRNA sequences despite their importance in the formation of granular cryoconite (Langford *et al.*, 2010) lends them as candidate keystone taxa or ecosystem engineers, echoing the agglomeration of desert soil particles by cyanobacterial exudates (West, 1990) often cited as a classical example of ecosystem engineering (Jones *et al.*, 1994). In this study, the weighting of intraset correlations between metabolite profiles and T-RFs matched by cyanobacterial clones (Table S2) supports the contention for their roles as autogenic ecosystem engineers. Furthermore, the close relation of primary production and respiration rates in cryoconite does imply the modulation of resource provision by cryoconite primary producers (Anesio *et al.*, 2009; Hodson *et al.*, 2010; Edwards *et al.*, 2011) at the process level. Overall, this lends further support to the notion that cryoconite ecosystems may be analogous to cold-region microbial mats (Edwards *et al.*, 2013a,b,c) in

that *Cyanobacteria* lend a structural component while diverse *Proteobacteria* sequences are numerically dominant (Varin *et al.*, 2010, 2012).

In conclusion, the combined application of T-RFLP, FT-IR and pyrosequencing of 16S rRNA genes to investigate the ecology of cryoconite habitats on alpine and Arctic glaciers demonstrates that there are clear differences in bacterial community structure and composition of metabolite profiles of cryoconites sampled from each region. It is likely that these regional variations will influence cryoconite ecosystem functionality, including supraglacial carbon cycling (Anesio *et al.*, 2009) and ice–microorganism-albedo feedbacks (Takeuchi, 2002). Considering the climate sensitivity and interactions of alpine and other mid-latitude, high-altitude region glaciers with human societies, the presence of distinctive bacterial communities on alpine glaciers merits further exploration. Finally, despite these differences, our comparative approach reveals commonalities in cryoconite ecosystems, thus providing insights into life in the glacial biome. In particular, these include the dominance of proteobacterial-affiliated OTUs over cyanobacterial-affiliated OTUs and the global prevalence of a few locally dominant taxa in cryoconite. When combined with the links between community structure and metabolite profiles, the data presented imply the importance of the metabolic versatility associated with the *Proteobacteria*, or the role of *Cyanobacteria* in aggregating cryoconite debris as key agents in the functionality of alpine and Arctic cryoconite ecosystems.

Acknowledgements

All field workers (AE, AJH, AMA, BP, BS, KH and SMER) are grateful for the operational support provided by Nick Cox and Rick Atkinson at NERC Arctic Research Station, Ny Ålesund, and the Alpine Forschungstelle Obergurgl (AFO) for hosting alpine fieldwork. This work was facilitated by grants to AE from the Society for General Microbiology (PFRV 10/4), the Aberystwyth University Research Fund and the Natural Environment Research Council (NE/K000942/1), and NERC funds to AMA and AJH (NERC NE/D007321/1); and a grant to BS (AFO Forschungsförderung 'GLAC.LIFE'). Finally, we thank three anonymous reviewers for their considered comments, and Kirsty Dougal for assistance with SRA.

References

Anderson MJ (2001) A new method for non-parametric multivariate analysis of variance. *Austral Ecol* **26**: 32–46.

Anderson MJ & Willis TJ (2003) Canonical analysis of principal coordinates: a useful method of constrained ordination for ecology. *Ecology* **84**: 511–525.

Anesio AM, Hodson AJ, Fritz A, Psenner R & Sattler B (2009) High microbial activity on glaciers: importance to the global carbon cycle. *Glob Change Biol* **15**: 955–960.

Anesio AM, Sattler B, Foreman C, Telling J, Hodson A, Tranter M & Psenner R (2010) Carbon fluxes through bacterial communities on glacier surfaces. *Ann Glaciol* **51**: 32–40.

Barnett TP, Adam JC & Lettenmaier DP (2005) Potential impacts of a warming climate on water availability in snow-dominated regions. *Nature* **438**: 303–309.

Bayley WS (1891) Mineralogy and petrography. *Am Nat* **25**: 138–146.

Blackwood CB, Hudleston D, Zak DR & Buyer JS (2007) Interpreting ecological diversity indices applied to terminal restriction fragment length polymorphism data: insights from simulated microbial communities. *Appl Environ Microbiol* **73**: 5276–5283.

Braak CJFT (1986) Canonical correspondence analysis: a new eigenvector technique for multivariate direct gradient analysis. *Ecology* **67**: 1167–1179.

Cameron K, Hodson AJ & Osborn AM (2012a) Carbon and nitrogen biogeochemical cycling potentials of supraglacial cryoconite communities. *Polar Biol* **35**: 1375–1393.

Cameron KA, Hodson AJ & Osborn AM (2012b) Structure and diversity of bacterial, eukaryotic and archaeal communities in glacial cryoconite holes from the Arctic and the Antarctic. *FEMS Microbiol Ecol* **82**: 254–267.

Caporaso JG, Kuczynski J, Stombaugh J *et al.* (2010) QIIME allows analysis of high-throughput community sequencing data. *Nat Methods* **7**: 335–336.

Christner BC, Kvitko BH & Reeve JN (2003) Molecular identification of bacteria and eukarya inhabiting an Antarctic cryoconite hole. *Extremophiles* **7**: 177–183.

Desmet WH & Vanrompus EA (1994) Rotifera and Tardigrada from some cryoconite holes on a Spitsbergen (Svalbard) glacier. *Belg J Zool* **124**: 27–37.

Dougal K, Harris PA, Edwards A, Pachebat JA, Blackmore TM, Worgan HJ & Newbold CJ (2012) A comparison of the microbiome and metabolome of different regions of the equine hindgut. *FEMS Microbiol Ecol* **82**: 642–652.

Edwards A, Anesio AM, Rassner SM *et al.* (2011) Possible interactions between bacterial diversity, microbial activity and supraglacial hydrology of cryoconite holes in Svalbard. *ISME J* **5**: 150–160.

Edwards A, Douglas B, Anesio AM, Rassner SM, Irvine-Fynn TDL, Sattler B & Griffith GW (2013a) A distinctive fungal community inhabiting cryoconite holes on glaciers in Svalbard. *Fungal Ecol* **6**: 168–176.

Edwards A, Pachebat JA, Swain M *et al.* (2013b) A metagenomic snapshot of taxonomic and functional diversity in an alpine glacier cryoconite ecosystem. *Environ Res Lett* **8**: 035003.

Edwards A, Rassner SM, Anesio AM *et al.* (2013c) Contrasts between the cryoconite and ice-marginal bacterial communities of Svalbard glaciers. *Polar Res* **32**: 19468.

Elliott GN, Worgan H, Broadhurst D, Draper J & Scullion J (2007) Soil differentiation using fingerprint Fourier

transform infrared spectroscopy, chemometrics and genetic algorithm-based feature selection. *Soil Biol Biochem* **39**: 2888–2896.

Fierer N, Bradford MA & Jackson RB (2007) Toward an ecological classification of soil bacteria. *Ecology* **88**: 1354–1364.

Foreman CM, Sattler B, Mikucki JA, Porazinska DL & Priscu JC (2007) Metabolic activity and diversity of cryoconites in the Taylor Valley, Antarctica. *J Geophys Res* **112**: G04S32.

Fountain AG, Tranter M, Nylen TH, Lewis KJ & Mueller DR (2004) Evolution of cryoconite holes and their contribution to meltwater runoff from glaciers in the McMurdo Dry Valleys, Antarctica. *J Glaciol* **50**: 35–45.

Franzetti A, Tatangelo V, Gandolfi I *et al.* (2013) Bacterial community structure on two alpine debris-covered glaciers and biogeography of *Polaromonas* phylotypes. *ISME J* **7**: 1483–1492.

Frisvad JC, Andersen B & Thrane U (2008) The use of secondary metabolite profiling in chemotaxonomy of filamentous fungi. *Mycol Res* **112**: 231–240.

Gidman EA, Stevens CJ, Goodacre R, Broadhurst D, Emmett B & Gwynn-Jones D (2006) Using metabolic fingerprinting of plants for evaluating nitrogen deposition impacts on the landscape level. *Glob Change Biol* **12**: 1460–1465.

Gribbon PWF (1979) Cryoconite holes on Sermikavask, West Greenland. *J Glaciol* **22**: 177–181.

Hamilton TL, Peters JW, Skidmore ML & Boyd ES (2013) Molecular evidence for an active endogenous microbiome beneath glacial ice. *ISME J* **7**: 1402–1412.

Hell K, Edwards A, Zarsky J *et al.* (2013) The dynamic bacterial communities of a melting High Arctic glacier snowpack. *ISME J* **7**: 1814–1826.

Hodson A, Anesio AM, Ng F *et al.* (2007) A glacier respires: quantifying the distribution and respiration CO_2 flux of cryoconite across an entire Arctic supraglacial ecosystem. *J Geophys Res* **112**: 9.

Hodson AJ, Anesio AM, Tranter M *et al.* (2008) Glacial ecosystems. *Ecol Monogr* **78**: 41–67.

Hodson A, Cameron K, Bøggild C, Irvine-Fynn T, Langford H, Pearce D & Banwart S (2010) The structure, biogeochemistry and formation of cryoconite aggregates upon an Arctic valley glacier; Longyearbreen, Svalbard. *J Glaciol* **56**: 349–362.

Huws SA, Kim EJ, Lee MRF *et al.* (2011) As yet uncultured bacteria phylogenetically classified as *Prevotella*, *Lachnospiraceae* incertae sedis and unclassified *Bacteroidales*, *Clostridiales* and *Ruminococcaceae* may play a predominant role in ruminal biohydrogenation. *Environ Microbiol* **13**: 1500–1512.

Irvine-Fynn TDL, Bridge JW & Hodson AJ (2011) *In situ* quantification of supraglacial cryoconite morpho-dynamics using time-lapse imaging: an example from Svalbard. *J Glaciol* **57**: 651–657.

Jangid K, Whitman W, Condron L, Turner BL & Williams MA (2013) Progressive and retrogressive ecosystem development coincide with soil bacterial community change in a dune system under lowland temperate rainforest in New Zealand. *Plant Soil* **367**: 235–247.

Jarvis RM, Broadhurst D, Johnson H, O'Boyle NM & Goodacre R (2006) PYCHEM: a multivariate analysis package for python. *Bioinformatics* **22**: 2565–2566.

Johnson HE, Broadhurst D, Kell DB, Theodorou MK, Merry RJ & Griffith GW (2004) High-throughput metabolic fingerprinting of legume silage fermentations via fourier transform infrared spectroscopy and chemometrics. *Appl Environ Microbiol* **70**: 1583–1592.

Jones CG, Lawton JH & Shachak M (1994) Organisms as ecosystem engineers. *Oikos* **69**: 373–386.

Kaltenborn BP, Nellemann C & Vistnes II (2010) *High Mountain Glaciers and Climate Change – Challenges to Human Livelihoods and Adaptation*. United Nations Environment Programme, GRID-Arendal., Arendal.

Kim SJ, Shin SC, Hong SG *et al.* (2012) Genome Sequence of *Janthinobacterium* sp. Strain PAMC 25724, isolated from alpine glacier cryoconite. *J Bacteriol* **194**: 2096.

Kohshima S, Seko K & Yoshimura Y (1993) Biotic acceleration of glacier melting in Yala Glacier, Langtang region, Nepal Himalaya. *Snow and Glacier Hydrology, Proceedings of the Kathumandu Symposium, IAHS Publication* **208**: 309–316.

Langford H, Hodson A, Banwart S & Bøggild C (2010) The microstructure and biogeochemistry of Arctic cryoconite granules. *Ann Glaciol* **51**: 87–94.

Langford H, Hodson A & Banwart S (2011) Using FTIR spectroscopy to characterise the soil mineralogy and geochemistry of cryoconite from Aldegondabreen glacier, Svalbard. *Appl Geochem* **26**(Suppl): S206–S209.

Legendre P & Anderson MJ (1999) Distance based Redundancy Analysis: testing multispecies responses in multifactorial ecological experiments. *Ecol Monogr* **69**: 1–24.

Liu WT, Marsh TL, Cheng H & Forney LJ (1997) Characterization of microbial diversity by determining terminal restriction fragment length polymorphisms of genes encoding 16S rRNA. *Appl Environ Microbiol* **63**: 4516–4522.

Margesin R, Zacke G & Schinner F (2002) Characterization of heterotrophic microorganisms in alpine glacier cryoconite. *Arct Antarct Alp Res* **34**: 88–93.

McIntyre NF (1984) Cryoconite hole thermodynamics. *Can J Earth Sci* **21**: 152–156.

Nobles LH (1960) Glaciological Investigations, Nunatarssuaq ice ramp, north west Greenland. Vol. Research Report 66 (US Army CoE, Snow Ice and Permafrost Research Establishment).

Oerlemans J, Giesen RH & van den Broeke MR (2009) Retreating alpine glaciers: increased melt rates due to the accumulation of dust (Vadret da Morteratsch, Switzerland). *J Glaciol* **55**: 729–736.

Pautler BG, Dubnick A, Sharp MJ, Simpson AJ & Simpson MJ (2013) Comparison of cryoconite organic matter composition from Arctic and Antarctic glaciers at the molecular-level. *Geochim Cosmochim Acta* **104**: 1–18.

Petit JR, Jouzel J, Raynaud D *et al.* (1999) Climate and atmospheric history of the past 420,000 years from the Vostok ice core, Antarctica. *Nature* **399**: 429–436.

Philippot L, Andersson SGE, Battin TJ, Prosser JI, Schimel JP, Whitman WB & Hallin S (2010) The ecological coherence of high bacterial taxonomic ranks. *Nat Rev Microbiol* **8**: 523–529.

Philippot L, Tscherko D, Bru D & Kandeler E (2011) Distribution of high bacterial taxa across the chronosequence of two alpine glacier forelands. *Microb Ecol* **61**: 303–312.

Prosser JI (2012) Ecosystem processes and interactions in a morass of diversity. *FEMS Microbiol Ecol* **81**: 507–519.

Säwström C, Mumford P, Marshall W, Hodson A & Laybourn-Parry J (2002) The microbial communities and primary productivity of cryoconite holes in an Arctic glacier (Svalbard 79°N). *Polar Biol* **25**: 591–596.

Scullion J, Elliott GN, Huang WE *et al.* (2003) Use of earthworm casts to validate FT-IR spectroscopy as a "sentinel" technology for high-throughput monitoring of global changes in microbial ecology: the 7th international symposium on earthworm ecology Cardiff, Wales, 2002. *Pedobiologia* **47**: 440–446.

Shiklomanov I (1993) World freshwater resources. *Water in Crisis: A Guide to the World's Fresh Water Resources* (Gleick PH, ed.), pp. 13–24. Oxford University Press, New York, NY.

Simon C, Wiezer A, Strittmatter AW & Daniel R (2009) Phylogenetic diversity and metabolic potential revealed in a glacier ice metagenome. *Appl Environ Microbiol* **75**: 7519–7526.

Sogin ML, Morrison HG, Huber JA *et al.* (2006) Microbial diversity in the deep sea and the underexplored "rare biosphere". *P Natl Acad Sci USA* **103**: 12115–12120.

Steinbock O (1936) Cryoconite holes and their biological significance. *Zeitschrift fur Gletscherkunde* **24**: 1–12.

Stibal M, Lawson EC, Lis GP, Mak KM, Wadham JL & Anesio AM (2010) Organic matter content and quality in supraglacial debris across the ablation zone of the Greenland ice sheet. *Ann Glaciol* **51**: 1–8.

Stibal M, Sabacka M & Zarsky J (2012a) Biological processes on glacier and ice sheet surfaces. *Nat Geosci* **5**: 771–774.

Stibal M, Telling J, Cook J, Mak KM, Hodson A & Anesio AM (2012b) Environmental controls on microbial abundance and activity on the Greenland ice sheet: a multivariate analysis approach. *Microb Ecol* **63**: 74–84.

Takeuchi N (2002) Optical characteristics of cryoconite (surface dust) on glaciers: the relationship between light absorency and the property of organic matter contained in the cryoconite. *Ann Glaciol* **34**: 409–414.

Takeuchi N, Kohshima S & Seko K (2001a) Structure, formation, and darkening process of albedo-reducing material (cryoconite) on a Himalayan glacier: a granular algal mat growing on the glacier. *Arct Antarct Alp Res* **33**: 115–122.

Takeuchi N, Kohshima S, Goto-Azuma K & Koerner R (2001b) Biological characteristics of dark colored material (cryoconite) on Canadian Arctic glaciers (Devon and Penny ice caps). *Mem Natl Inst Polar Res* **54**: 495–505.

Takeuchi N, Nishiyama H & Li Z (2010) Structure and formation process of cryoconite granules on Ürümqi glacier No. 1, Tien Shan, China. *Ann Glaciol* **51**: 9–14.

Telling J, Anesio AM, Tranter M *et al.* (2012a) Controls on the autochthonous production and respiration of organic matter in cryoconite holes on high Arctic glaciers. *J Geophys Res* **117**: G01017.

Telling J, Stibal M, Anesio AM *et al.* (2012b) Microbial nitrogen cycling on the Greenland Ice Sheet. *Biogeosci Discuss* **9**: 2431–2442.

Tieber A, Lettner H, Bossew P, Hubmer A, Sattler B & Hofmann W (2009) Accumulation of anthropogenic radionuclides in cryoconites on Alpine glaciers. *J Environ Radioact* **100**: 590–598.

Tindall BJ, Brambilla E, Steffen M, Neumann R, Pukall R, Kroppenstedt RM & Stackebrandt E (2000) Cultivatable microbial biodiversity: gnawing at the Gordian knot. *Environ Microbiol* **2**: 310–318.

Turnbaugh PJ & Gordon JI (2008) An invitation to the marriage of metagenomics and metabolomics. *Cell* **134**: 708–713.

Varin T, Lovejoy C, Jungblut AD, Vincent WF & Corbeil J (2010) Metagenomic profiling of Arctic microbial mat communities as nutrient scavenging and recycling systems. *Limnol Oceanogr* **55**: 1901–1911.

Varin T, Lovejoy C, Jungblut AD, Vincent WF & Corbeil J (2012) Metagenomic analysis of stress genes in microbial mat communities from Antarctica and the high Arctic. *Appl Environ Microbiol* **78**: 549–559.

Vasyurenko ZP & Frolov AF (1986) Fatty acid composition of bacteria as a chemotaxonomic criterion. *J Hyg Epidemiol Microbiol Immunol* **30**: 287–293.

West NE (1990) *Structure and Function of Microphytic Soil Crusts in Wildland Ecosystems of Arid to Semi-arid Regions*. Academic Press, Waltham, MA, pp. 179–223.

Wharton RA, Mckay CP, Simmons GM & Parker BC (1985) Cryoconite holes on glaciers. *Bioscience* **35**: 499–503.

Wittebolle L, Marzorati M, Clement L *et al.* (2009) Initial community evenness favours functionality under selective stress. *Nature* **458**: 623–626.

Xu Y, Simpson AJ, Eyles N & Simpson MJ (2009) Sources and molecular composition of cryoconite organic matter from the Athabasca Glacier, Canadian Rocky Mountains. *Org Geochem* **41**: 177–186.

Yallop ML, Anesio AM, Perkins RG *et al.* (2012) Photophysiology and albedo-changing potential of the ice algal community on the surface of the Greenland ice sheet. *ISME J* **6**: 2302–2313.

Zarsky JD, Stibal M, Hodson A *et al.* (2013) Large cryoconite aggregates on a Svalbard glacier support a diverse microbial community including ammonia-oxidizing archaea. *Environ Res Lett* **8**: 035044.

Supporting Information

Additional Supporting Information may be found in the online version of this article:

Fig. S1. Abundance distribution of T-RFs demonstrating intraset correlations ≥ 0.1 in value (green) in environmental axes 1–3 against metabolite profiles vs. background T-RFs (i.e. not selected in CCA; red) relative abundances at the regional scale (a: SV; b: GR; c: AT).

Table S1. Taxonomic and relative abundance data for pyrosequencing reads.

Table S2. Environmental axis weightings for T-RFs in a summary CCA model of T-RF influence on FT-IR metabolite profiles.